International Journal of Engineering Trends and Technology
ISSN: 2231 – 5381 / https://doi.org/10.14445/22315381/IJETT-V70I11P225

Volume 70 Issue 11, 232-239, November 2022

Original Article

Comparative Study of Drag Reduction of Square-back Vehicle Geometry using Steady blowing and Fluidic Oscillators Method

Thanh-Long Phan[1], Tien Thua Nguyen[2]

[1,2]*Faculty of Transportation Mechanical Engineering, University of Science and Technology, The University of Danang, Danang City, Vietnam*

[1]*Corresponding Author : ptlong@dut.udn.vn*

Received: 22 August 2022 Revised: 09 November 2022 Accepted: 16 November 2022 Published: 26 November 2022

Abstract *- A 3D finite volume method numerical simulation was conducted on the square-back Ahmed model to compare the drag reduction capability and energy efficiency between steady blowing and fluidic oscillators flow control techniques. A parametric study was carried out with various operational conditions of actuators, i.e., the jet angle and velocity of the steady blowing method and the input mass flow rate of each actuator for a fluid oscillator. Applying both active flow control methods leads to an aerodynamic drag reduction of the Ahmed model. Furthermore, the analysis of the near-wake structure revealed a recovery of static pressure on the rear surface of the model. The control energy efficiency was then studied, and the results showed the best efficiency of 8.04 % for the steady blowing method at momentum coefficient $C_\mu = 2.21 \times 10^{-3}$ and jet angle $\theta = 30^o$. For the fluidic oscillator cases, each actuator had a maximum energy efficiency of 10.88 % at the input mass flow rate of 1.5 kg/h.*

Keywords *- Active Flow Control, CFD, Drag Reduction, Fluidic Oscillator, Steady Blowing Method.*

1. Introduction

To solve the problems of climate change and environmental protection, various modes of transport, especially ground vehicles, must reduce fuel consumption. This can be achieved partly by reducing the vehicle's aerodynamic drag, which accounts for more than 60% of its total drag at highway speeds [1]. The total drag of a vehicle is dominated by the absence of pressure recovery in large wake structures at the rear surface, which increases the aerodynamic drag. Many researchers have used different passive and active flow control methods to delay flow separation and reduce the recirculation zone at the rear-facing surface, thereby reducing aerodynamic drag. A passive flow control device is often added to the vehicle and interacts with freestream flow without needing an external power source [2].

Conversely, additional energy is supplied for active flow control devices to modify the outer flow field. For flow control devices, low control methods aim to gain more saved propulsion power than the supplied energy input. Seifert and coworkers placed an array of their developed actuators mounted inside a circular cylinder on the top edge of the back side of truck trailers. A drag reduction of 20 % was achieved by increasing back pressure [3]. Taubert and Wygnanski used an oscillating jet in combination with the flap plates to reduce the drag of a truck model [4]. In addition, an active flow control system using the Coanda effect has been mounted on all four edges of the rear surface of a simple truck model [5]. This study has shown a maximum drag reduction of 15% with optimized flow control device configuration.

Some other studies, such as F. Aloui et al. [6], have used the synthetic jet actuator positioned at the top edge of the 25° Ahmed rear slant surface. The experimental results have shown that aerodynamic drag is significantly reduced by about 10% when optimal control is applied. The advantage of this actuator concept is that it is compact and easy to control, but the jet flow velocity is limited. Besides, an experimental and numerical study by McNally et al. [27], which used a microjet actuator to control the flow behind a miniature car model, showed a reduction drag of nearly 3% compared to vehicles without active flow control.

In active flow control methods, various studies have been conducted using steady blowing [8–16] and fluid oscillators [17–21] as actuators. Englar et al. employed a steady-blowing jet on the vehicle's rear surface, obtaining a drag reduction of more than 30 % [8]. Rouméas [9] and Wassen [10] conducted numerical simulations using steady blowing on the square-back Ahmed model and obtained a drag reduction of around

17–29 %. This active flow control method is also used to reduce the aerodynamic drag of passenger cars. Experimental results showed a drag reduction of 12% on a commercial van model with a steady microjet array on the vehicle's rear end [11].

Similarly, Baek et al. [12] showed that the drag coefficient could be reduced by about 7.5 % on the realistic car DriAver model using this method. According to those studies, a steady-blowing actuator significantly reduces the vehicle's aerodynamic drag. However, this flow control technique requires significant energy inputs, which reduces the beneficial effect.

In order to overcome the shortcomings of the steady-blowing flow technique, a device called a fluidic oscillator is used as a flow control actuator to delay separation at the rear end of the vehicle, thereby reducing aerodynamic drag. This device generates a sweeping jet output from a steady flow input thanks to internal feedback channels. These feedback channels partially redirect the outlet flow, forcing the incoming jet into the opposing wall. The frequency of the sweeping jet depends on the device's geometry, flow rate, and input flow [22].

One advantage of fluidic oscillators is that they can impact a larger flow region for a given energy input than other active flow control methods. Recently, several experimental studies have been conducted to evaluate the potential of using fluidic oscillators for vehicle drag reduction. Woszidlo et al. used fluidic oscillators on a 1:10 simplified truck model with base flaps [17]. Dirk Wieser and coworkers investigated the effect of this device on a DriAver vehicle model [18]. These studies showed a drag reduction of up to 20 % compared to the reference case.

Although the above studies have shown that the fluidic oscillator flow control technique is more efficient than the steady blowing technique for reducing the vehicle aerodynamic drag due to the delay of flow separation, these studies are carried out on various vehicle models. Thus, a systematic comparison of the aerodynamic drag reduction capabilities between these two flow control techniques has not been widely studied under different operating conditions. Therefore, in this paper, a numerical study is performed to compare the ability to reduce drag and control energy efficiency of these two actuator types, then select the most suitable flow control technique for aerodynamic drag reduction. The simulation was carried out on the square-back Ahmed model, as the wake characteristics are very similar to that of vans and trucks [23]. The steady-blowing jets and fluidic oscillators are mounted on the upper edge of the model's rear surface. The control parameters are modified to investigate the effectiveness of these two active flow control techniques.

2. Computational Setup

2.1. Ahmed Vehicle Models

The Ahmed car model was first proposed in 1984 [23] and is used to study the relationship between the rear-end design and aerodynamic drag. The wake structure and the aerodynamic drag depend highly on the rear slant angle φ. In this study, the Ahmed vehicle model is used with a slant angle of 90°, which is the typical shape of the truck and bus. The geometry and dimensions of the square-back Ahmed model are shown in Figure 1.

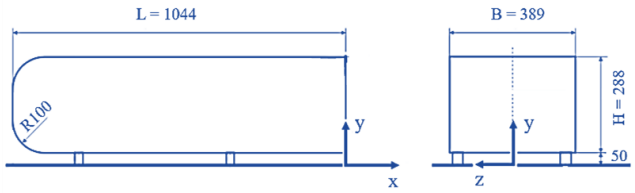

Fig. 1 The square-back Ahmed model with dimensions in mm

A steady-blowing jet is applied through a small continuous slot at the top edge of the rear surface of the model. The thickness of this slot is h = 1 mm. The blowing jet angle θ is defined as the angle formed by the jet direction and the longitudinal axis (Figure 2). This numerical study changes this angle to investigate the most optimal jet angle for the steady-blowing technique.

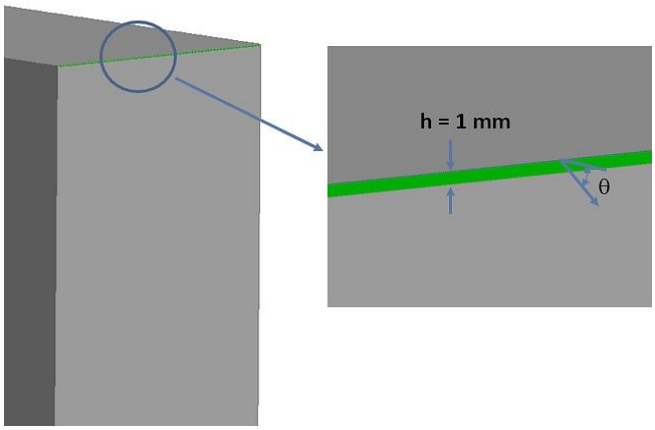

Fig. 2 Schematic of the steady-blowing simulation

In order to simulate the steady-blowing jet, a uniform velocity V_j boundary condition is applied at a continuous slot behind the Ahmed vehicle model. The momentum coefficient C_μ of the steady jet actuation is defined as

$$C_\mu = \frac{h}{H}\left(\frac{V_j}{V_o}\right)^2 \quad (1)$$

where H is Ahmed's model height, and V_o is inflow velocity.

In the case of fluidic oscillators, the devices are placed on the upper edge of the rear surface of the vehicle, as shown in Figure 3. The distance between the fluid oscillators is Δz = 36 mm.

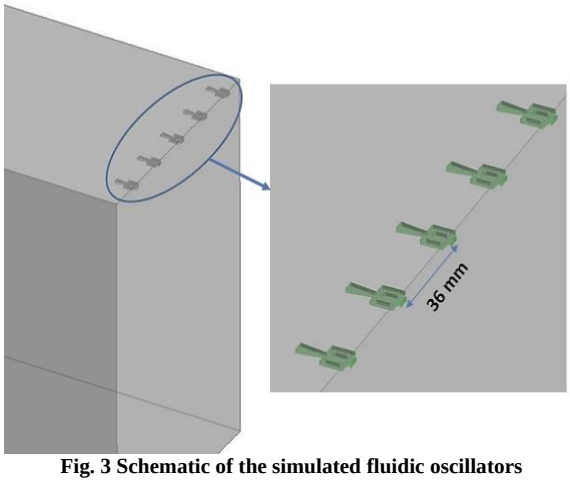

Fig. 3 Schematic of the simulated fluidic oscillators

For the current numerical study, the geometry of the fluidic oscillator is determined from previous experimental studies [24], presented in Figure 4. The momentum coefficient C_μ of the fluidic oscillator actuator is defined by Equation 2:

$$C_\mu = \frac{2\dot{m}^2}{\rho_0^2 A A_j N V_0^2} \quad (2)$$

where m is the inlet mass flow rate of the single actuator, ρ_o is the density of freestream air, A is the vehicle frontal area, A_j is the area of each actuator, and N is the number of fluidic oscillators on the vehicle.

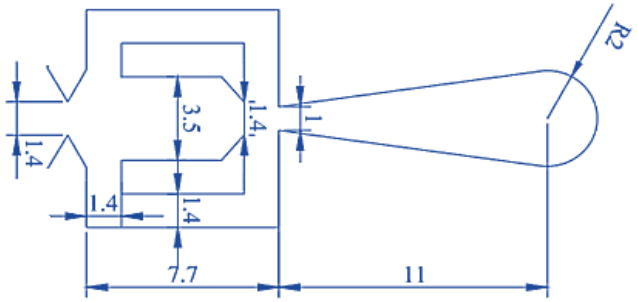

Fig. 4 Dimensions of the fluidic oscillator in mm

2.2. Computational Mesh and Method

The computational domain is rectangular with dimensions of 25H, 5H, and 3H, where H = 288 mm –the height of the Ahmed model (Figure 5). The domain behind the model was extended to 18 body height to prevent the impact of outflow boundary conditions on near-wake development. A uniform velocity V_0 = 30 m/s was applied to the domain inlet condition. At the outlet of the domain, a pressure boundary condition is used. A slip condition is imposed on the domain side and top walls. The bottom wall and Ahmed model are both given the no-slip boundary condition. Finally, the XY plane (z = 0) is known as the symmetry condition.

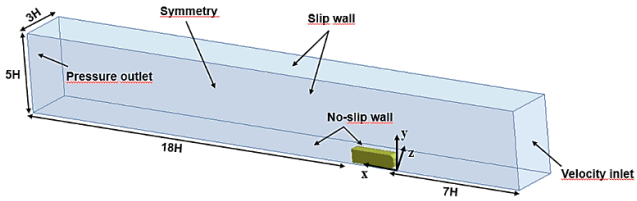

Fig. 5 Computational domain and Boundary conditions for simulation

The numerical modeling is done using commercial software ANSYS 2020 [25]. A CAD model of the computational domain is created using the Design Modeler module. The domain is manually split into multi-block regions, and the ANSYS ICEM module generates a hexagonal mesh. This hexagonal mesh type is of higher quality and requires fewer computing resources than the unstructured mesh type. A mesh refinement is needed in the region near the Ahmed body. In addition, the vicinity of the continuous slot at the rear surface of the model where the actuators are installed has been more refined (Fig 6).

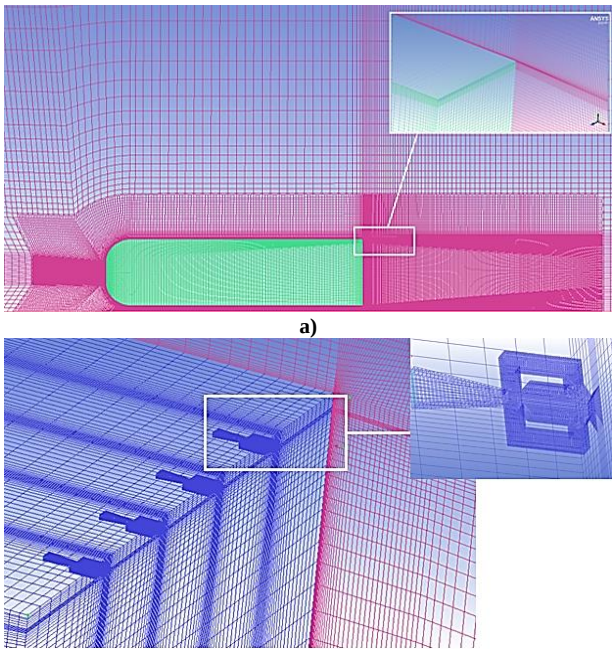

a)

b)

Fig. 6 Computational mesh for simulation: (a) steady blowing; (b) fluidic oscillator

Figure 7 presents a mesh independence study of drag coefficient C_d in the case of unactuated flow with four levels of mesh element number, i.e., 0.5, 1, 2.5, and 4.5 million elements. The results showed that the change of C_d was less significant when the number of mesh elements exceeded 2.5 million. In this case, a drag coefficient of C_d = 0.241 was obtained. This value is slightly lower than the experimental value (C_d = 0.25) from the work of Ahmed et al. [23]. This can be explained by the removal of the four legs of the Ahmed model in this numerical study.

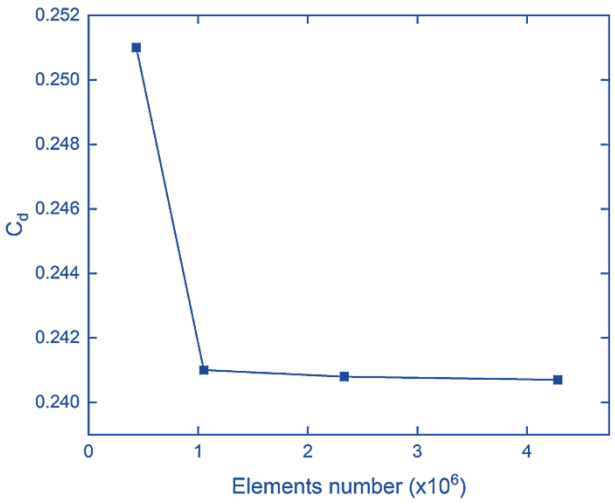

Fig. 7 Mesh independent test

The finite volume solver ANSYS Fluent 2020 was used to conduct the simulations presented in this work, with three cases: unactuated flow, control flow using a steady blowing jet, and control flow with fluid oscillator actuators. The URANS k - ω SST turbulence model was used and specified with time step size $\Delta t = 10^{-4}$ s in 3000-time steps to predict the flow field accurately. This turbulence model is widely used because it meets both the requirements of the solution accuracy and computational resources [26]. For the pressure-velocity coupling, the well-known SIMPLEC scheme was employed.

3. Numerical Results

The drag reduction capability of the steady-blowing jet and fluidic oscillator techniques were evaluated under several different operating conditions. For the steady blowing method, the jet angle was varied with five different values, $\theta = 0^o$, 15^o, 30^o, 45^o, and 60^o, as described in Figure 2. The jet velocity was proportional to inflow velocity, $V_j = A.V_o$, and the coefficient A was modified in the range of 0.15 to 1.5. The momentum coefficient C_μ of the actuator varied between 7.7 x 10^{-5} and 7.8 x 10^{-3}. In the case of the fluidic oscillator technique, the input mass flow rate of each actuator varied from 0.5 kg/h to 3 kg/h, which corresponded to a momentum coefficient C_μ in the range of 6.9 x 10^{-5} to 2.5 x 10^{-3}.

The time-averaged velocity field is presented in Fig. 8 with a steady blowing jet of momentum coefficient C_μ = 2.21 x 10^{-3} and jet angle $\theta = 30^o$. The results showed that the jet outflow from a continuous slot could emulate the base flaps' ability to reduce aerodynamic drag by delaying the separation in shear layers. The wake structures behind the Ahmed model can be modified by applying the steady-blowing jet, leading to a reduction in drag.

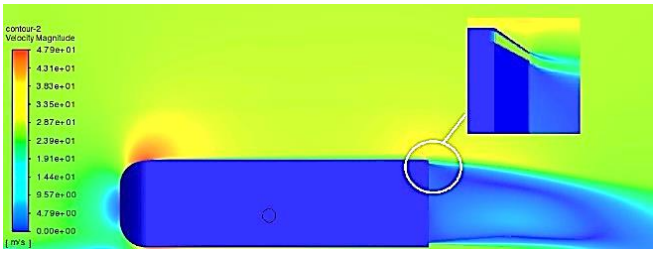

Fig. 8 Contour of velocity field with steady blowing jet

Similarly, Figure 9 shows the outflow jet from the fluidic oscillators installed on the top edge of Ahmed's rear surface. From the figure, it can be seen that one benefit of the fluidic oscillator is the sweeping of a large region of flow. This can be seen as equivalent to using a continuously steady blowing jet but with less input flow, improving control energy efficiency.

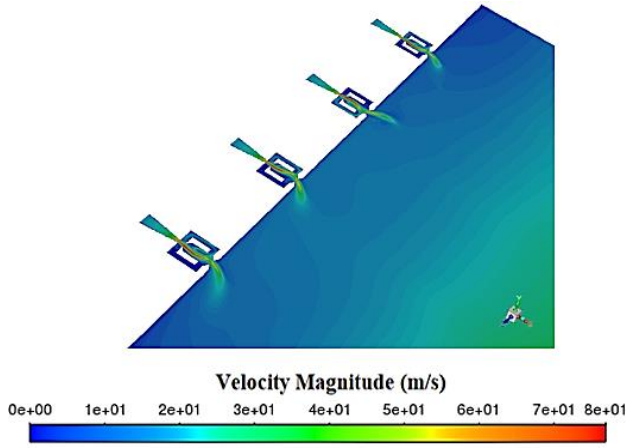

Fig. 9 The outflow jet from fluid oscillators installed on the Ahmed model

The evaluation of the drag coefficient with two control flow techniques in different operating conditions is shown in Figure 10.

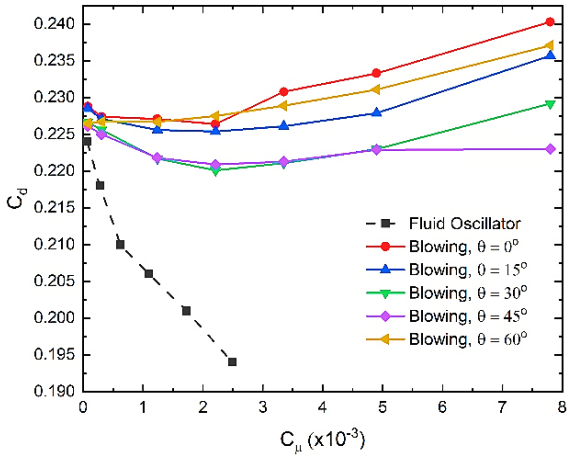

Fig. 10 Aerodynamic drag coefficient evolution as a function of momentum coefficient

In addition, to evaluate the reduction of the drag coefficient of the Ahmed vehicle in the cases of different jet angles θ and coefficients of momentum C_μ, the parameter ΔC_d is proposed as follows:

$$\Delta C_d = 100 \frac{C_d - C_{d_o}}{C_{d_o}} \ (\%) \qquad (3)$$

where C_d is the drag coefficient of the model-equipped active flow control actuators under various operation conditions, and C_{do} is the drag coefficient of the model in the reference case (C_{do} = 0.241). The percentage change of the drag coefficient ΔC_d of the Ahmed model in different cases according to the coefficient of momentum C_μ is shown in Figure 11.

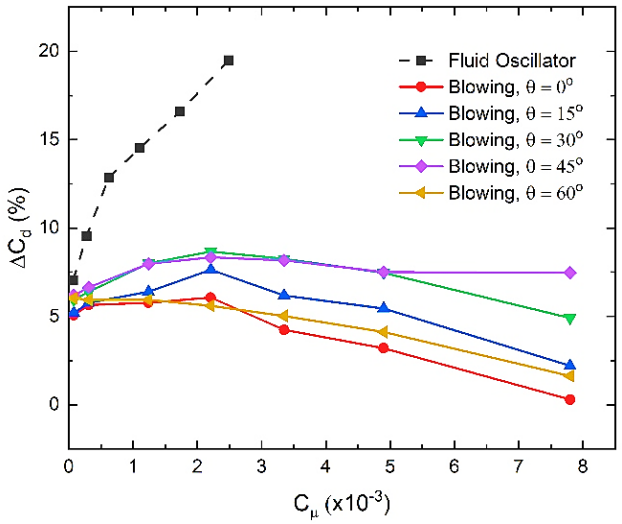

Fig. 11 Percentage change of aerodynamic drag coefficient evolution as a function of momentum coefficient

The numerical results presented in Figures 10 and 11 reveal that for the steady blowing technique, a minimum drag coefficient is obtained at jet angles θ = 30° and θ = 45°. Rouméas et al. [8] also found a similar result and identified that the optimal jet angle for a steady-blowing actuator was 45°. In addition, the Ahmed model's drag reduction gradually increases from the momentum coefficient C_μ = 0.077 x 10^{-3} and reaches a maximum value at C_μ = 2.21 x 10^{-3}. As C_μ increases to a value of 7.8 x 10^{-3}, the drag reduction gradually decreases. The maximum drag reduction of the Ahmed model with a steady-blowing actuator is 8.67% at a jet angle θ = 30° and the momentum coefficient C_μ = 2.21 x 10^{-3}. For the model with a fluidic oscillator actuator, the drag reduction is proportional to the input mass flow rate of actuators.

The effect of the active flow actuators on the distribution of pressure coefficient C_p on the rear surface of the model is illustrated in Figure 12. The static pressure in this location is responsible for most of the model aerodynamic drag. The results in Figure 12 reveal that in the two control cases (Figures 12b and c), the high-pressure region is larger than the reference case without control (Figure 12a). It demonstrates that the static pressure is well recovered behind the model with control flow actuators, thereby reducing the aerodynamic drag (Figure 10). For the fluidic oscillator case with input mass flow rate m = 1.5 kg/h (Figure 12c), the maximum pressure coefficient C_p = -0.16 is achieved, consistent with the highest drag reduction.

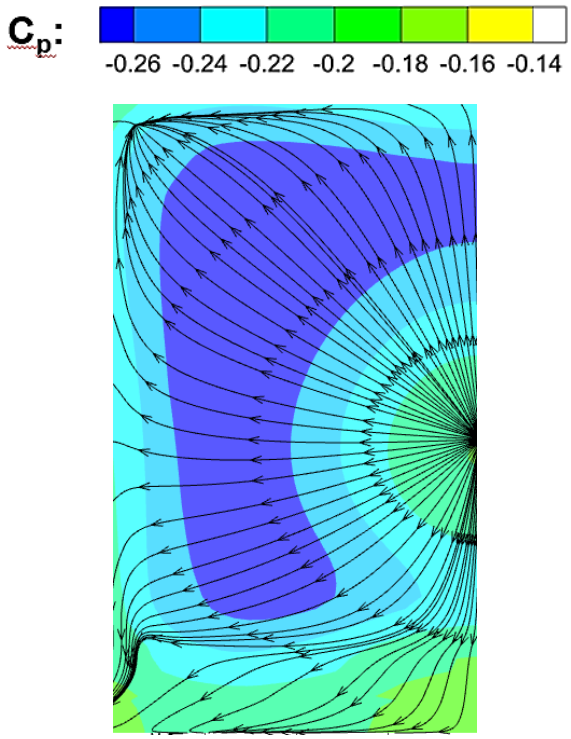

a)

b)

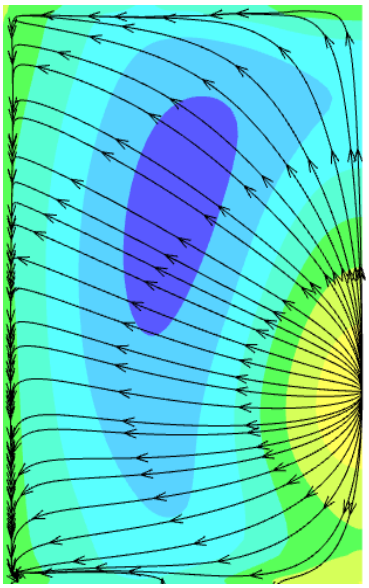

c)

Fig. 12 Pressure coefficient distribution on the rear model surface for three different cases: a) reference case, b) steady blowing θ = 30°, c) fluidic oscillator m = 1.5 kg/h

The streamline and velocity fields at the symmetry plane (z = 0) in different cases are presented in Figure 13. The development of wake structures affects the pressure distribution on the rear surface of the model, which in turn, changes the aerodynamic drag. Figure 13 reveals the formation of recirculation zones in the near-wake flow behind the model. These vortices form suction regions on wake low and create a low-pressure zone on the rear surface. Applying the active flow control method, i.e., the steady blowing jet in Figure 13b and fluidic oscillators in Figure 13c, modified the wake flow topology compared to the reference flow without control. The introduction of momentum from the actuators into flow caused a shear effect that induced an inclination of streamlines and reduced the wake section. In addition, momentum applied from the actuators into the flow tended to reduce the size of recirculation zones in the wake flow and displaced these zones further away from the rear surface of the model.

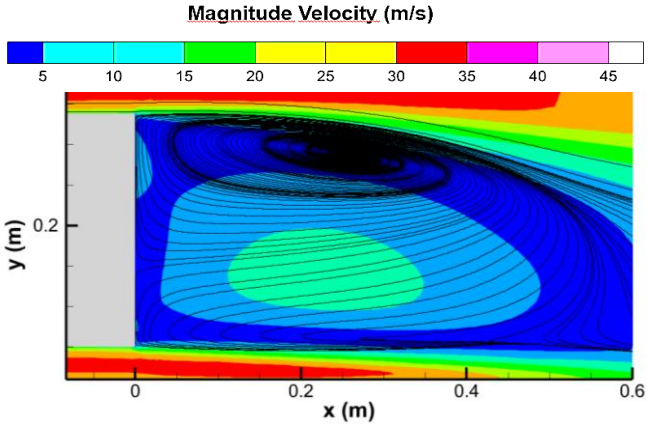

a)

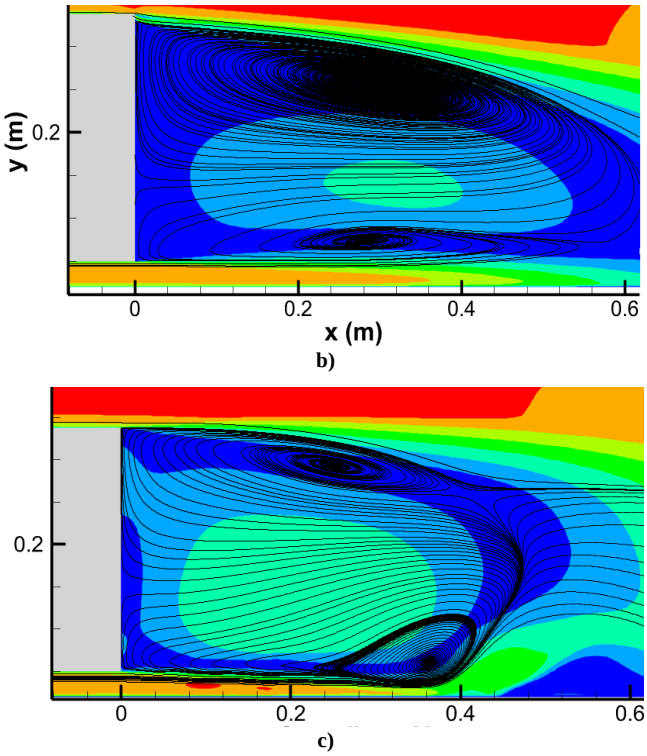

b)

c)

Fig. 13 Contours of magnitude velocity with streamlines in the symmetry plane for three different cases: a) reference flow, b) steady blowing θ = 30°, c) fluidic oscillator m = 1.5 kg/h

4. Control Efficiency

As mentioned in the previous section, both active flow control techniques demonstrate the ability of model drag reduction. The maximum reduction for the steady-blowing jet is 8.67%, whereas the largest drag reduction of 19.5% was obtained with the fluidic oscillator method. This is a very significant reduction compared to other flow control methods. However, since both techniques are active flow control types, they require an external energy source to generate the output jets. Therefore, a simple calculation formula proposes to evaluate the control method's energy efficiency. The propulsion power needed to overcome aerodynamic drag for unactuated flow is given by:

$$\mathbf{P_{D_0} = \frac{1}{2}\rho C_{d_o} A V_o^3\ (W)} \qquad (4)$$

The power supply for the actuators is described as:

$$\mathbf{P_j = \frac{1}{2} m V_j^2\ (W)} \qquad (5)$$

The energy efficiency of the control methods is then defined as:

$$\eta = \frac{(P_{D_0} - P_D) - P_j}{P_{D_0}} = \frac{\Delta C_d}{C_{d0}} - \frac{m V_j^2}{\rho C_{d0} A V_0^3} \qquad (6)$$

From Equation 6, the energy efficiency of both control methods obtained from numerical parametric studies was calculated, and the results are presented in Figure 14.

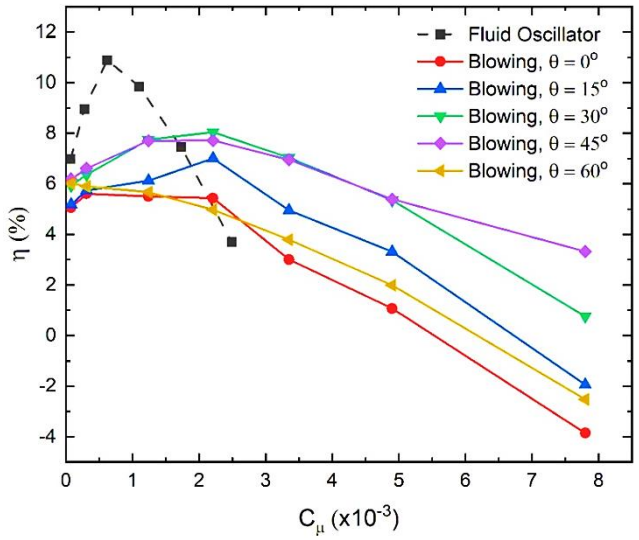

Fig. 14 Control energy efficiency evolution as a function of momentum coefficient

The results in Figure 14 reveal that in most cases of a steady-blowing jet, the energy efficiency is positive, and the maximum value of 8.04 % was obtained at a jet angle $\theta = 30^o$ and a momentum coefficient $C_\mu = 2.21 \times 10^{-3}$. In these conditions, the saved power is greater than the supplied power for the flow control actuators. However, as the momentum coefficient C_μ was increased, a reduction in energy efficiency could be noticed. At $C_\mu = 7.8 \times 10^{-3}$, this efficiency became negative (with jet angle $\theta = 0^o$, 15^o and 60^o). In these cases, the flow control systems lead to an increment in the operational power requirement of the model.

For the case of fluidic oscillators, the maximum energy efficiency of 10.88 % was achieved at an input mass flow rate of m = 1.5 kg/h. At high inlet mass flow rates, the drag reduction increased but also caused a decrease in energy efficiency, which means that more external energy is required for the actuator systems.

5. Conclusion

A reduction in aerodynamic drag on a square-back Ahmed model using steady-blowing and fluidic oscillator techniques was studied through numerical simulation. For the steady blowing method, the jet velocity and angle were varied, and a maximum drag reduction of 8.67 % was obtained at a momentum coefficient $C_\mu = 2.21 \times 10^{-3}$ and jet angle $\theta = 30^o$. In the case of the fluidic oscillator technique, the drag reduction was proportional to the input mass flow rate for actuators. In addition, the introduction of momentum from the actuator output jet into flow modified the near-wake structure and caused pressure recovery on the model's rear surface.

The best efficiency of 8.04 % was achieved using the steady blowing method, a momentum coefficient $C_\mu = 2.21 \times 10^{-3}$ and jet angle $\theta = 30^o$. Meanwhile, in several control cases, the control efficiency was negative, which means that the external energy required for actuators is greater than the saved energy in reducing the aerodynamic drag. The best control energy efficiency of the model with the fluidic oscillator systems was 10.88 %, with an input mass flow rate of 1.5 kg/h for each actuator. The numerical results in this study demonstrate that the fluidic oscillator method is suitable for vehicle aerodynamics drag reduction.

Funding Statement

The Ministry of Education and Training funds this research, grant number B2020-DNA-03.

References

[1] W. Hucho, "*Aerodynamics of Road Vehicles*," Society of Automotive Engineers, Inc, Warrendale, Pa, pp. 85-89, 1998.

[2] P. Shakti, S. Patel and S. Patel, "Commercial Vehicle Aerodynamic Drag Reduction: (Tipper Truck)," *International Journal of Engineering Trends and Technology*, vol. 44, no. 4, pp. 170-178, 2017. Crossref, https://doi.org/ 10.14445/22315381/IJETT-V44P234

[3] A. Seifert, O. Stalnov and D. Sperber, "Large Trucks Drag Reduction Using Active Flow Control," The Aerodynamics of Heavy Vehicles II: Trucks, Buses and Trains in Lecture Notes in Applied and Computational Mechanics, Berlin, Germany: *Springer*, vol. 41, pp. 115-133, 2007. Crossref, https://doi.org/ 10.1007/978-3-540-85070-0_10

[4] L. Taubert and I. Wygnanski, "Preliminary Experiments Applying Active Flow Control to a 1/24th Scale Model of a Semi-Trailer Truck," The Aerodynamics of Heavy Vehicles II: Trucks, Buses and Trainsin Lecture Notes in Applied and Computational Mechanics. Berlin, Germany: *Springer*, vol. 41, pp. 105-113, 2007. Crossref, https://doi.org/10.1007/978-3-540-85070-0_9

[5] E. D. Manosalvas, D. T. Economon, C. Othmer and A. Jameson, "Computational Design of Drag Diminishing Active Flow Control Systems for Heavy Vehicles," *in Proc. 8th AIAA Flow Control Conference*, pp. 1-15, 2016. Crossref, https://doi.org/10.2514/6.2016-4082

[6] N. Tounsi, R. Mestiri, L. Keirsbulck, H.Oualli, S. Hanchi and F. Aloui, "Experimental Study of Flow Control on Bluff Body using Piezoelectric Actuators," *Journal of Applied Fluid Mechanics*, vol. 9, no. 2, pp. 827-838, 2016. Crossref, https://doi.org/10.18869/ACADPUB.JAFM.68.225.24488

[7] Ashraf E. Abdu-Razak, Ehsan F. Abbas and Tahseen A. Tahseen, "The Effect of Vibration on the Heat Transfer from a Vertical Plate: A Review," *SSRG International Journal of Thermal Engineering*, vol. 6, no. 3, pp. 1-5, 2020. Crossref, https://doi.org/10.14445/23950250/IJTE-V6I3P101

[8] R. J. Englar, "Improved Pneumatic Aerodynamics for Drag Reduction, Fuel Economy, Safety and Stability Increase for Heavy Vehicles," *SAE Technical Paper*, vol. 724, pp. 1-11, 2005. Crossref, https://doi.org/10.4271/2005-01-3627

[9] M. Rouméas, P. Gilléron and A. Kourta, "Analysis and Control of the Near-Wake Flow Over a Square-Back Geometry," *Computers & Fluids*, vol. 38, no. 1, pp. 60-70, 2009 Crossref, https://doi.org/10.1016/j.compfluid.2008.01.009

[10] E. Wassen, S. Eichinger and F. Thiele, "Simulation of Active Drag Reduction for a Square-back Vehicle," Active Flow Control II in Notes on Numerical Fluid Mechanics and Multidisciplinary Design. Berlin, Germany: *Springer*, vol. 108, pp. 241-255, 2010. Crossref, https://doi.org/10.1007/978-3-642-11735-0_16

[11] J. J. Cerutti, C. Sardu, G. Cafiero and G. Iuso, "Active Flow Control on a Square-back Road Vehicle," *Fluids*, vol. 5, pp. 55-82, 2020.

[12] S-W. Baek, S. W. Lee, "Aerodynamic Drag Reduction on a Realistic Vehicle Using Continuous Blowing," *Microsystem Technologies*, vol. 26, pp. 11-23, 2020. Crossref, https://doi.org/10.1007/s00542-019-04355-w

[13] R. Mestiri, A. Ahmed-Bensoltane, L. Keirsbulck, F. Aloui and L. Labraga, "Active Flow Control at the Rear End of a Generic Car Model Using Steady Blowing," *Journal of Applied Fluid Mechanics*, vol. 7, no. 4, pp. 565-571,2014.

[14] R. P. Littlewood and M. A. Passmore, "Aerodynamic Drag Reduction of a Simplified Squareback Vehicle Using Steady Blowing," *Experiments in Fluids*, vol. 53, pp. 519-529, 2012. Crossref, https://doi.org/10.1007/s00348-012-1306-4

[15] Z. Mohamed-Kassim and A. Filippone,"Fuel Savings on a Heavy Vehicle Via Aerodynamic Drag Reduction," *Transportation Research Part D: Transport and Environment*, vol.15, no. 5, pp. 275-284,2010. Crossref, https://doi.org/10.1016/j.trd.2010.02.010

[16] W. Cui, H. Zhu, C. Xia and Z. Yang,"Comparison of Steady Blowing and Synthetic Jets for Aerodynamic Drag Reduction of a Simplified Vehicle," *Procedia Engineering*, vol. 126, pp. 388-392, 2015. Crossref, https://doi.org/10.1016/j.proeng.2015.11.224

[17] H-J. Schmidt, R. Woszidlo, C. N. Nayeri and C.O. Paschereit, "Experimental Investigation of the Flow Field behind a Bluff Body Equipped with Fluidic Oscillators," *in Prof. 53rd AIAA Aerospace Sciences Meeting*, pp. 1-16, 2015. Crossref, https://doi.org/10.2514/6.2015-0786

[18] D. Wieser, H. Lang, C. Nayeri and C. Paschereit, "Manipulation of the Aerodynamic Behavior of the DrivAer Model with Fluidic Oscillators," *SAE International Journal of Passenger Vehicle Systems*, vol. 8, no. 2, pp. 687-702, 2015. Crossref, https://doi.org/10.4271/2015-01-1540

[19] H-J. Schmidt, R. Woszidlo, C. N. Nayeri and C.O. Paschereit, "The Effect of Flow Control on the Wake Dynamics of a Rectangular Bluff Body in Ground Proximity," *Experiments in Fluids*, vol. 59, pp. 107-123, 2018. Crossref, https://doi.org/10.1007/s00348-018-2560-x

[20] M. Metka and J. W. Gregory, "Drag Reduction on the 25-deg Ahmed Model Using Fluidic Oscillators," *Journal of Fluids Engineering*, vol. 137, pp. 1-8, 2015. Crossref, https://doi.org/10.1115/1.4029535

[21] M. Metka, "Flow Control on the Ahmed Body Vehicle Model Using Fluidic Oscillators," *in Prof. the ASME 2013 International Mechanical Engineering Congress and Exposition IMECE2013*, pp. 1-10, 2013. Crossref, https://doi.org/10.1115/IMECE2013-67343

[22] F. Oz and K. Kara, "Jet Oscillation Frequency Characterization of a Sweeping Jet Actuator," *Fluids*, vol. 5, no. 2, pp. 72-88,2020. Crossref, https://doi.org/10.3390/fluids5020072

[23] S. R. Ahmed, G. Ramm and G. Faltin, "Some Salient Features of the Time Average Ground Vehicle Wake," *SAE Technical Paper*, pp. 1-34, 1984. Crossref, https://doi.org/10.4271/840300

[24] K. Kara, D. Kim and P. J. Morris, "Flow-Separation Control using Sweeping Jet Actuator," *AIAA*, vol. 56, no. 11, pp. 4604-4613, 2018. Crossref, https://doi.org/10.2514/1.J056715

[25] The Ansys Website, 2022. [Online]. Available:https://www.ansys.com/

[26] F. R. Menter, "Two-Equation Eddy-Viscosity Turbulence Models for Engineering Applications," *AIAA*, vol. 32, no. 8, pp. 1598 – 1605, 1994. Crossref, https://doi.org/10.2514/3.12149

[27] J. McNally, E. Fernandez, G. Robertson, R. Kumar, K. Taira, F. Alvi, Y. Yamaguchi and K. Murayama, "Drag Reduction on a Flat-Back Ground Vehicle with Active Flow Control," *Journal of Wind Engineering and Industrial Aerodynamics*, vol. 145, pp. 292-303, 2015. Crossref, https://doi.org/10.1016/j.jweia.2015.03.006